# Early stages of oxidation of Ti3AlC2 ceramics

Song, G.M.; Pei, Y.T.; Sloof, W.G.; Li, S.B.; Hosson, J.Th.M. De; Zwaag, S. van der

*Published in:*
Materials Chemistry and Physics

*DOI:*
10.1016/j.matchemphys.2008.06.038



*Publication date:*
2008

Materials Chemistry and Physics 112 (2008) 762–768

Contents lists available at ScienceDirect

Materials Chemistry and Physics

journal homepage: www.elsevier.com/locate/matchemphys

# Early stages of oxidation of $Ti_3AlC_2$ ceramics

G.M. Song[a,b,*], Y.T. Pei[c], W.G. Sloof[a], S.B. Li[d], J.Th.M. De Hosson[c], S. van der Zwaag[b]

[a] Department of Materials Science and Engineering, Delft University of Technology, Mekelweg 2, 2628 CD Delft, The Netherlands
[b] Fundamentals of Advanced Materials, Faculty of Aerospace Engineering, Delft University of Technology, Kluyverweg 1, 2629 SH Delft, The Netherlands
[c] Department of Applied Physics, The Netherlands Materials Innovation Institute, University of Groningen, Nijenborgh 4, 9747 AG Groningen, The Netherlands
[d] Materials Engineer Center, Beijing Jiaotong University, Beijing 100044, PR China

ARTICLE INFO

*Article history:*
Received 26 February 2008
Received in revised form 5 May 2008
Accepted 15 June 2008

*Keywords:*
$Ti_3AlC_2$
Oxidation
$Al_2O_3$
$TiO_2$

ABSTRACT

The nucleation and growth of oxide scale at the early stages of oxidation of $Ti_3AlC_2$ ceramics was studied via oxidizing at 1100 °C in air for short times (≤900 s). The nucleation of nanosized $Al_2O_3$ particles mainly occurs at the ledges of the fractured lamellar $Ti_3AlC_2$ grains as well as on the {0 0 0 1} basal surfaces. The $Al_2O_3$ nuclei mainly grow along these ledges to form oxide strings, and then spread on the terraces and the {0 0 0 1} basal surfaces. An oxide layer consisting predominantly of nanosized α-$Al_2O_3$ forms after oxidizing for 180 s. The formation of lenticular hexagonal pores in $Ti_3AlC_2$ grains is attributed to the faster consumption of Ti, Al and C atoms along ⟨1 1 $\bar{2}$ 0⟩ direction than along ⟨0 0 0 1⟩ direction. With further oxidation, rutile-$TiO_2$ particles form on top of the α-$Al_2O_3$ layer, and grow to form a rutile-$TiO_2$ layer. Further oxidation leads to the formation of pores underneath the primary α-$Al_2O_3$ layer. In this porous layer both $Al_2O_3$ and $TiO_2$ were present with a preference for $Al_2O_3$ to stay adjacent to the inward moving interface of $Ti_3AlC_2$ substrate.



## 1. Introduction

Ternary carbide $Ti_3AlC_2$, belonging to the family of layered ternary compounds notated as $M_{n+1}AX_n$ with $n = 1–3$, where M is an early transition metal, A is an A-group element and X is C or N, has recently received extensive attention because it has a remarkable and attractive mechanical performance [1–8] and consequently is a potential candidate for high temperature structural applications. Our recent work on $Ti_3AlC_2$ ceramic has demonstrated that $Ti_3AlC_2$ has also an excellent crack healing ability at high temperatures [9]. In fact microcracks on the surface can be repaired by the oxidation product ($Al_2O_3 + TiO_2$) of $Ti_3AlC_2$ via a high temperature oxidation process of which the early stage is of particular relevance.

The oxidation behavior of $Ti_3AlC_2$ as such has been studied in the past few years [2,10–14] as the moderate oxidation resistance is a major obstacle for many applications. The results of Barsoum et al. [10,11] about the oxidation of $Ti_3AlC_2$ revealed the formation of an $Al_2O_3$-rich striated layer adjacent to the $Ti_3AlC_2$ substrate. This striation was attributed to the demixing of a rutile-based ($Ti_{1-y}Al_yO_{2-y/2}$) layer [10,11] formed on the surface suggesting that the formation of the rutile-based ($Ti_{1-y}Al_yO_{2-y/2}$) layer preceded the formation of $Al_2O_3$ layer. The experimental validation for this hypothesis is lacking. Wang et al. [2,12] found that the oxide scale of $Ti_3AlC_2$ had a two-layer structure: an α-$Al_2O_3$ inner layer and a rutile-$TiO_2$ outer layer. The inner layer did adhere to the substrate and was more or less continuous, which accounted for an adequate oxidation resistance of $Ti_3AlC_2$. It was suggested that the formation of the α-$Al_2O_3$ layer was caused by the inward diffusion of oxygen through the outer $TiO_2$ layer rather than outward flow of Al [11]. However, as of to date no experimental evidence has been provided for this hypothesis. Detailed information about the early stages of the oxidation of $Ti_3AlC_2$ is lacking.

While it is obvious that the continuity of the first α-$Al_2O_3$ scale determines the oxidation resistance of $Ti_3AlC_2$ ceramics, the formation process of such oxide layer are not very clear because the previous researches mainly focused on the oxidation behaviors of long exposure time [2,10–14]. Especially, knowledge about the nucleation and growth of the initial oxides on the $Ti_3AlC_2$ surface is not available due to the absence of solid experimental evidence. Similarly, information about the early oxidation stages of other MAX phases, such as $Ti_3SiC_2$ [15], $Ti_2SnC$ [16], $Zr_3Al_3C_5$ [17], etc., is also lacking. Therefore, a thorough understanding of the oxidation reaction and microstructural evolution of the oxide scale at the early stages of oxidation of MAX materials is crucial not only for the improvement of the oxidation resistance of $Ti_3AlC_2$ bulk ceramics, but also for the microcrack healing process [9]. In this study, the nucleation and growth process of oxide scale at the early stages of oxidation of $Ti_3AlC_2$ ceramic at 1100 °C in air have been

* Corresponding author at: Department of Materials Science and Engineering, Delft University of Technology, Mekelweg 2, 2628 CD Delft, The Netherlands. Tel.: +31 15 2789459; fax: +31 15 2786730.
*E-mail address:* G.Song@tudelft.nl (G.M. Song).

0254-0584/$ – see front matter © 2008 Elsevier B.V. All rights reserved.
doi:10.1016/j.matchemphys.2008.06.038

scrutinized with scanning electron microscopy (SEM) and X-ray diffraction (XRD). The formation mechanism of the oxide scale is discussed.

## 2. Experimental procedures

A $Ti_3AlC_2$ bulk sample was prepared via an in situ solid–liquid reaction of Ti, Al and graphite powders under hot-pressing conditions. Detailed description of the preparation can be found elsewhere [9]. SEM observation on the final $Ti_3AlC_2$ sample showed that the $Ti_3AlC_2$ sample consists of lamellar grains with an average length of ~8 μm and an average thickness of ~2 μm. The highly polished $Ti_3AlC_2$ bar with a size of 32 mm × 2 mm × 3 mm was fractured into pieces of about 3 mm × 2 mm × 3 mm. These small samples with fresh fracture surfaces were placed in an air-loaded furnace at a preset temperature of 1100 °C for isothermal oxidation studies. The reason for choosing the samples with fracture surfaces rather than the conventional samples with flat polished surfaces is that some specific crystalline planes are usually present at fracture surfaces, which is suitable for the study of anisotropic characteristics of a crystal for some specific cases. This method provides a simple way for preparing single crystal with specific crystalline planes. Given the small dimensions of the samples and the good thermal conductivity of the material, the samples were expected to reach the furnace temperature of 1100 °C within several seconds. At the end of preset oxidizing times the samples were taken out from the furnace and rapidly cooled in air.

The morphologies of the oxidized fracture surfaces of these samples were studied via a scanning electron microscope (SEM, JSM 6500F and JSM 7500F, Japan) equipped with an energy dispersive spectroscope (EDS, Noran Pioneer 30 $mm^2$ Si(Li) detector) for chemical composition analysis. The operation voltage for EDS was 15 keV. The phases formed at the fracture surface upon oxidation were determined with an X-ray diffractometer (Bruker AXS D5005 XRD, Germany) using Cu Kα radiation under an operation voltage of 45 keV.

## 3. Results and discussion

### 3.1. Nucleation and growth of oxides on the fracture surface

No nanosized particles were observed on the fresh fracture surface of $Ti_3AlC_2$; see Fig. 1a. But after oxidizing the sample at 1100 °C for 20 s, nanosized particles, considered as the nuclei of the oxides form on the fracture surface. Some crystalline faces of the lamellar grains have more particles formed, and the other faces are almost particle free; see Fig. 1b and c. It is noteworthy that the oxide nuclei on the lateral surface of the lamellar grain prefer to align themselves along the ledges (Fig. 1b and c). Fig. 1c shows that the oxidized state of both crack surfaces of a partly cleaved grain is different from each other. The density of the oxide particle of surface A is higher than that of surface B. Cleavage of lamellar $Ti_3AlC_2$ grains occurs mainly parallel to the hexagonal basal (0 0 0 1) plane [1,2,9,18], i.e. along the interface between the octahedral $Ti_3C_2$ layer and Al layer due to the relative weaker cohesive strength between Ti atom layer and Al atom layer governed by the Ti–Al metallic bonding [19,20]. One can envision that one of the cleavage surfaces (i.e. basal (0 0 0 1) surface) has a terminal layer consisting of Al atoms only, while the other surface is end-capped with a $Ti_3C_2$ layer. Nuclei of aluminum oxides and titanium oxides perhaps form simultaneously on the two cleavage surfaces. The energy states of Al and Ti in $Ti_3AlC_2$ are different from those in pure Al and $TiC_x$. Nevertheless, we may approximately compare the chemical reactivity of Al and Ti atoms in $Ti_3AlC_2$ with oxygen using pure Al and TiC, based on the crystal structure of $Ti_3AlC_2$ that can be described as periodic planar stacking of sheets of edge-sharing $Ti_6C$ octahedral and close-packed Al atoms along the *c*-axis [1]. The Gibbs energies of the formation of $Al_2O_3$ with pure Al and the formation of TiO (or $TiO_2$) with Ti in $TiC_x$ are negative [21–23]. In detail, the Gibbs energy for $Al_2O_3$ formation upon the reaction of Al atom with per mole O at 1373 K is −413 kJ, and for $TiO_2$ formation upon TiC it is −28 kJ [22]. It is thus believed that the cleavage surface with Al terminal layer is more easily oxidized than that with a $Ti_3C_2$ layer on top. Therefore, more $Al_2O_3$ nuclei than $TiO_2$ nuclei may be expected to form. In theory it is possible for $Al_2O_3$ nuclei to form on the $Ti_2C_3$ basal plane, although

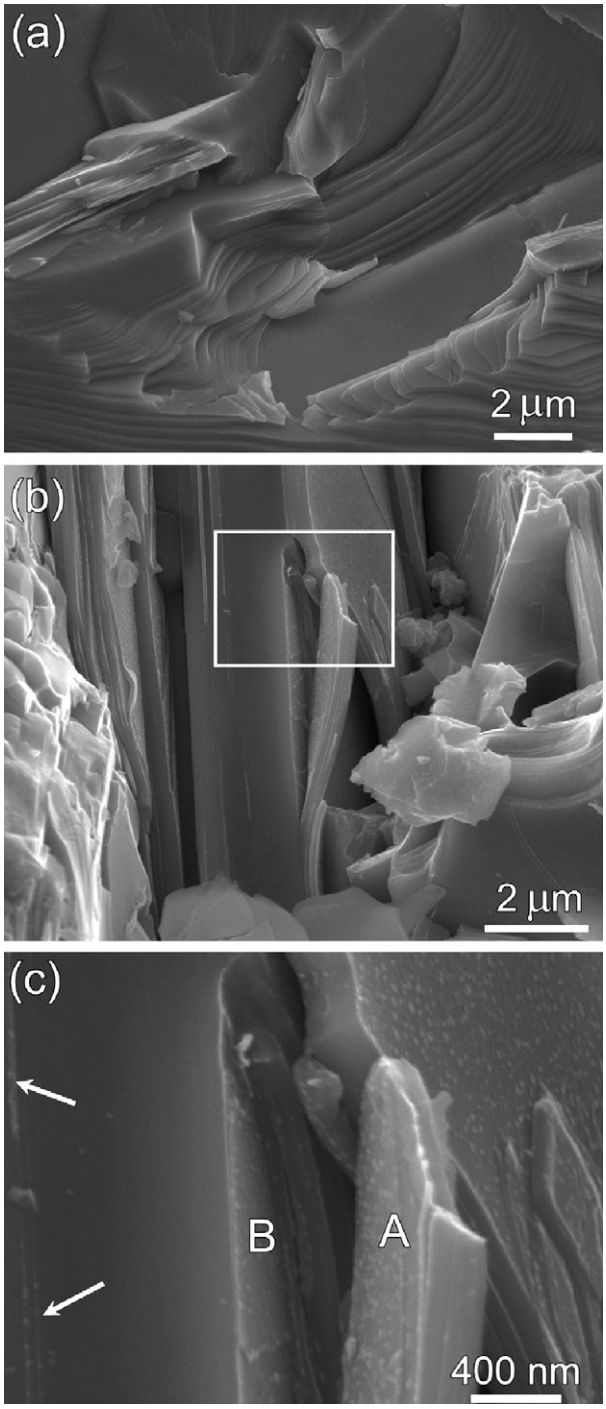


**Fig. 1.** SEM micrographs showing the fracture surface of $Ti_3AlC_2$ samples: (a) fresh fracture surface without any oxide particle; (b and c) nanosized oxide particles formed on the fracture surface after oxidized at 1100 °C for 20 s; (c) magnified micrograph of the area indicated by a box in (b). The oxidation of surface A of the cleavage is more severe than that of surface B. Arrows indicate the oxide particles aligned at the step edges on the lateral surface.

the diffusion of Al atoms through the $Ti_2C_3$ layer onto the outer surface may be relatively difficult compared to the diffusion of atomic Al along the basal plane. Alternatively, atomic Al can firstly diffuse internally along the basal plane to the ledges of the basal surface, and then diffuses from the ledges to the outside surface.

The oxides nuclei on the lateral faces of lamellar grains are mainly present at the ledges, and consequently form oxide strings,

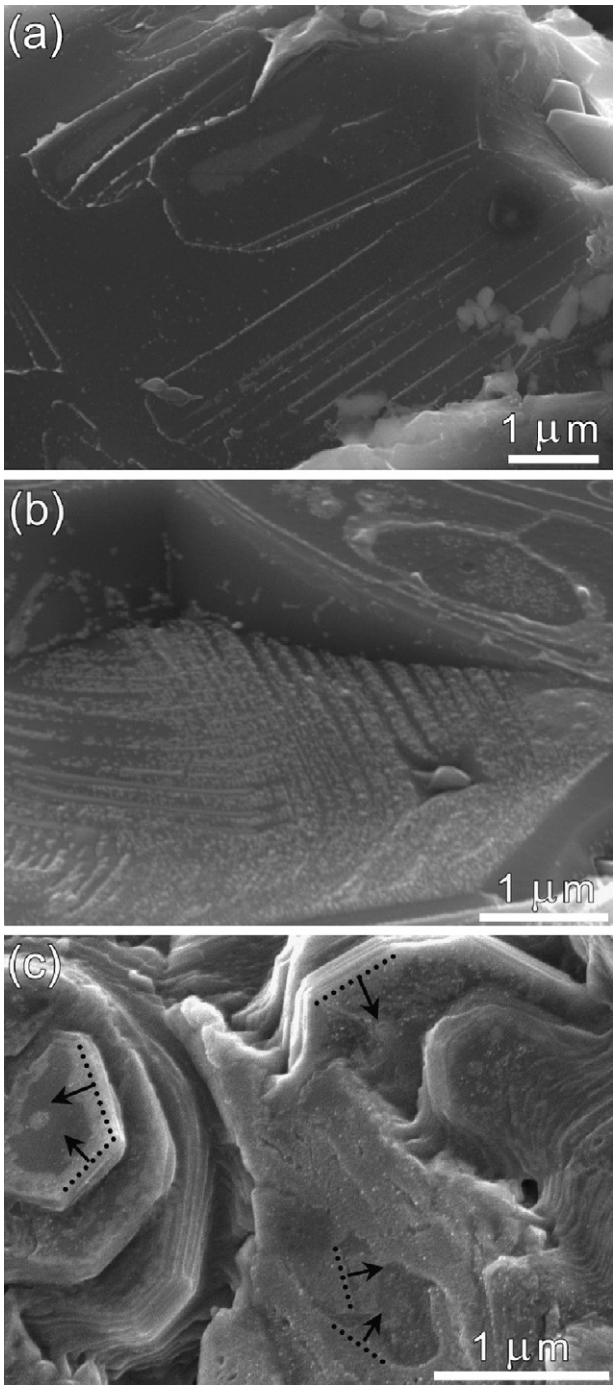


**Fig. 2.** Fracture surfaces oxidized at 1100 °C for (a) 20 s, (b) 60 s and (c) 180 s.

as indicated by arrows in Fig. 1b. The string-like morphology may be due to three factors: (1) the lateral surface of lamellar grain has a mixture of layered Al atom chains and $Ti_3C_2$ chains. The nuclei of $Al_2O_3$ certainly prefer to initiate along the Al atom planes; (2) the inner Al atoms easily diffuse to ledges along the basal plane, which makes the ledges be preferential sites for the nucleation by providing sufficient Al atoms; (3) compared with a smooth area, a step edge (rough area) has a high surface energy [24] and more-coordinated sites, which is beneficial for nucleation. These nuclei at the ledges align due to geometrical constraints and grow over the step terraces to form string-like morphology with time, as shown in Fig. 2a and b. The outward raised oxide particles reveal the volume expansion and outgrowth of the oxides at the initial oxidation stage of $Ti_3AlC_2$.

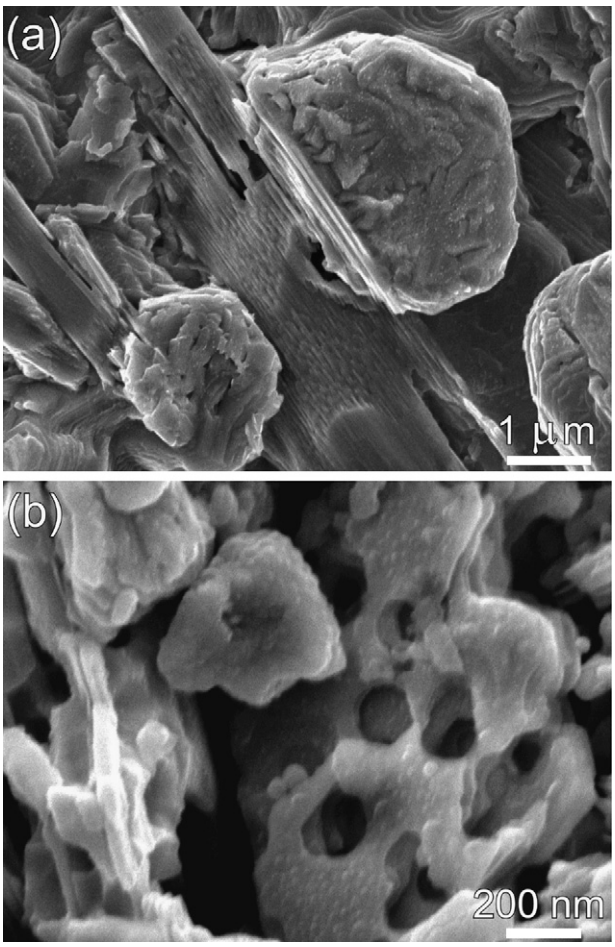


**Fig. 3.** Formation of hexagonal pores: (a) aligned as pits on the lateral surface after oxidized for 180 s and (b) lying on the basal plane of $Ti_3AlC_2$ grain oxidized for 360 s.

### 3.2. Formation of oxide scale on the fracture surface

The oxide nuclei grow and coalesce as the oxidation progresses, and finally a dense oxide scale forms on the fracture surface in about 180 s. Meanwhile, the fracture surface becomes rougher due to the formation of oxide particles, as shown in Fig. 2c. Ordered oxide particle arrays with an average thickness of 100 nm (see also Fig. 4a) on the basal surfaces of the lamellar grains are frequently observed. These arrays consist of nanosized semi-spherical oxide particles. As indicated by the dotted lines, the ordered arrays initiate mainly at the edges of the basal surfaces, and then spread to the central parts along specific crystalline orientations. XRD measurements do not detect the $Al_2O_3$ and $TiO_2$ phases on the surface oxidized for 180 s due to the very thin thickness of the oxide scale (~100 nm) and the strong influence from the underlying $Ti_3AlC_2$ substrate. EDS analysis shows that the Ti/Al atomic ratio is about 2.7 measured on the oxidized surface and slightly lower than the ratio of ~3 in the base $Ti_3AlC_2$. Meanwhile, oxygen is detected on the oxidized surface, which corresponds to a high $Al_2O_3$ content in the oxide scale. By using EDS, similar enrichment of Al on the oxidized $Ti_3AlC_2$ particles has been identified when $Ti_3AlC_2$ particles were exposed to air at 800 °C for 2 h [25]. As mentioned in Section 3.1, the oxide nuclei consist mainly of $Al_2O_3$ particles, and the outward diffusion of Al atoms from the sub-surface of $Ti_3AlC_2$ grains is faster than that

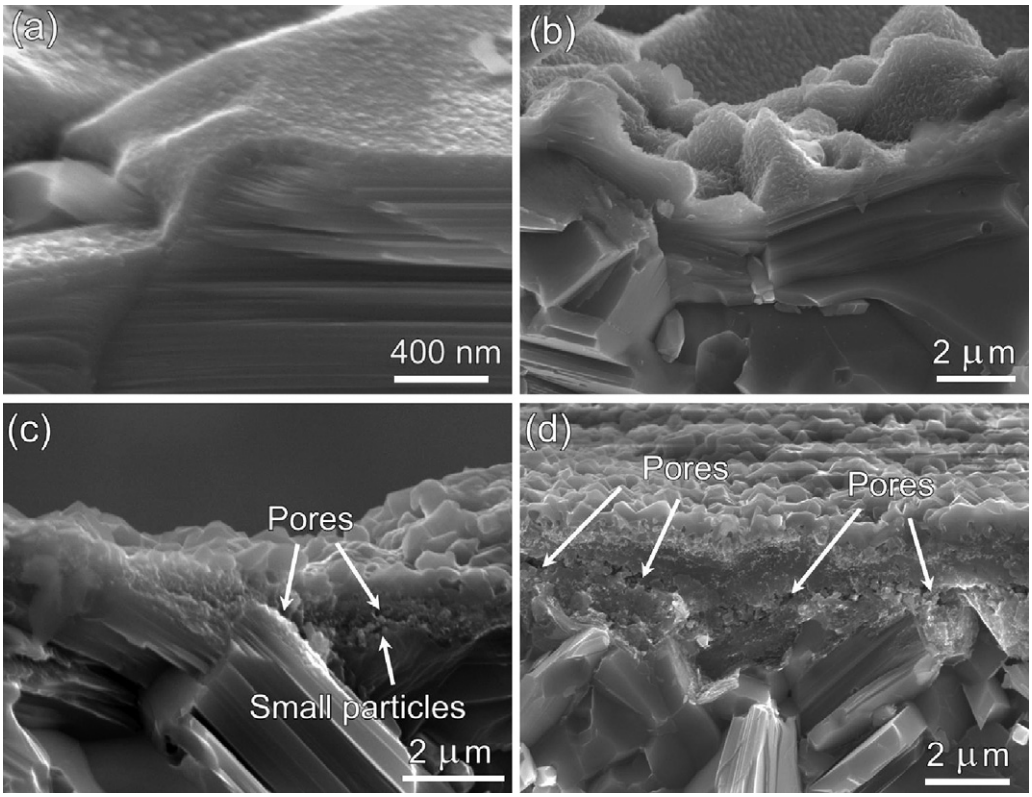


**Fig. 4.** Fracture cross-sections of oxidized $Ti_3AlC_2$ ceramics at 1100 °C for (a) 180 s; (b) 360 s; (c) 600 s; (d) 900 s.

of Ti atoms because the Ti–C bonding is more directional and strong, whereas the Ti–Al bonding is weaker [19,20]. Therefore, the initial oxide scale should contain predominantly α-$Al_2O_3$. Previous works of Wang et al. [2,12] and Lin et al. [26,27] show that the α-$Al_2O_3$ was still predominant in the oxide scale of $Ti_3AlC_2$ after oxidized at 1100 °C even up for 20 h, and only small amount of $TiO_2$ crystallites were observed at the $Al_2O_3$ grain boundaries or within the $Al_2O_3$ grains [26].

### 3.3. Formation of pores on the fracture surface

Small amounts of lenticular-pore chains are observed at the lateral surfaces of the lamellar grains oxidized for 180 s (Fig. 3a). The laminated hexagonal feature of the lenticular pores becomes clearer after oxidizing for 360 s (Fig. 3b). For its formation two hypotheses may be formulated: (1) the consumption rates of Al, Ti and C atoms along $\langle 1\,1\,\bar{2}\,0\rangle$ direction of $Ti_3AlC_2$ grain are faster than those along the $\langle 0\,0\,0\,1\rangle$ direction; (2) the consumption of Ti, Al and C atoms occur in a cooperative manner. The later explanation fits with the experimental results of Wang et al. about the absence of an Al depletion layer or Ti-rich layer in the $Ti_3AlC_2$ sub-scale area [12]. However, precise composition analysis of the $Al_2O_3/Ti_3AlC_2$ interface zone with transmission electron microscopy combining EDS showed the existence of very thin (50–100 nm) Al depletion layer adjacent to the interface [27]. It means that upon oxidation, first Al atoms diffuse outwards to the substrate surface to react with oxygen. Due to the depletion of Al atoms on the basal plane, the $Ti_3AlC_2$ lattices are distorted and become $Ti_3C_2$ separated by discontinuous micropores. Al atoms lie on specific planes in the lamellar $Ti_3AlC_2$ lattice, and thus the micropores are aligned. These pores provide fast channels for the inward diffusion of oxygen and the release of $CO_2$ or CO gas phase. Oxygen can first enter the vacancy layers to possibly form $Ti_3C_2O_y$ solid solution and oxidation of $Ti_3C_2O_y$ proceeds [13,28]. The whole oxidation process could be separated as two steps [13]:

$$4Ti_3AlC_2 + (2y+3)O_2 = 4Ti_3C_2O_y + 2Al_2O_3 \quad (1)$$

$$4Ti_3C_2O_y + (20-2y)O_2 = 12TiO_2 + 8CO_2 \quad (2)$$

Under low oxygen potential, CO rather than $CO_2$ might form. Such a coupled two-step oxidation process is most likely responsible for the formation of the aligned hexagonal pores in the lamellar $Ti_3AlC_2$ grains.

Wang and Zhou [13] found that the aligned pores existed at the oxidized surfaces of $Ti_3AlC_2$ powders after a thermal cycle treat-

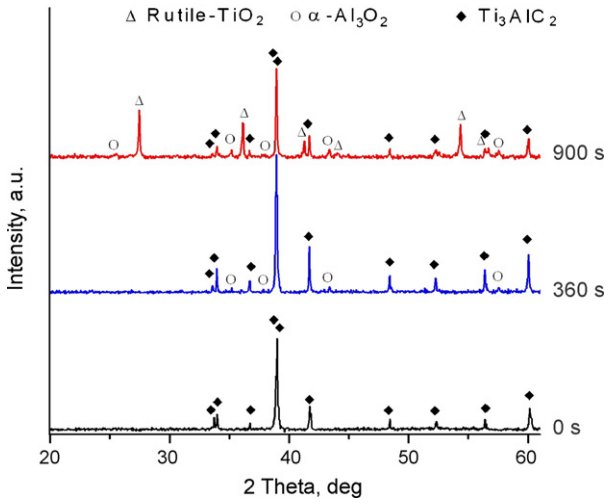


**Fig. 5.** XRD patterns of $Ti_3AlC_2$ oxidized at 1100 °C for 0 s, 360 s and 900 s, respectively.

ment from room temperature to 1460 °C in Ar containing 12 ppm oxygen. The oxidation rate of $Ti_3AlC_2$ under such a condition with extremely low oxygen content should be very low, and thus the oxidation status is analogous to the oxidation early stages. Our present observation also shows the existence of such micropores at the early stages for bulk $Ti_3AlC_2$ samples. The laminated hexagonal morphology of $Ti_3AlC_2$ grain itself has already been identified by scanning electron microscopy or transmission electron microscopy [1–3]. It is believed that such a morphology is caused by the relative higher growth rate of $\{1\,1\,\bar{2}\,0\}$ lateral plane of $Ti_3AlC_2$ grain than that of $\{0\,0\,0\,1\}$ basal plane. This hypothesis has been confirmed in $Ti_3SiC_2$, which has a similar hexagonal structure [29,30]. During the oxidation process (or hot-etching), reversibly, the depletion rate of atoms at $\{1\,1\,\bar{2}\,0\}$ lateral plane should be higher, and consequently, hexagonal lamellar pores form, which demonstrate the anisotropy of the oxidation rate of hexagonal $Ti_3AlC_2$ grain.

Although the fracture surface can be covered by a continuous $Al_2O_3$ oxide scale, small amount of pores disrupt the continuity of the scale and undoubtedly provide a faster path for the inward diffusion of oxygen. These pores are undesirable for oxidation resistance of $Ti_3AlC_2$ ceramics.

### 3.4. Growth of oxide scale on the fracture surface

Cross-sectional views of the oxidized fractured surfaces are shown in Fig. 4. After oxidation of 180 s, a thin continuous oxide scale with a thickness of about 100 nm covers the surface of the sample (Fig. 4a). When the oxidation time increases to 360 s, the oxide scale grows with fine faceted particles formed on top, and the thickness increases to about 300 nm (Fig. 4b). The faceted particles further grow and the oxide scale thickens with time. Small amounts of fine pores are observed underneath the oxide scale after oxidization for 600 s. These fine pores are adjacent to the unoxidized $Ti_3AlC_2$ substrate, indicated by arrows in Fig. 4c. After oxidation for 900 s, a developed porous layer formed underneath the primary $Al_2O_3$ layer. Within the porous layer there are loose particles ($TiO_2 + Al_2O_3$); see Fig. 4d. The size of the loose particles is about 50–200 nm, which is much smaller than that of the outer $TiO_2$ grains (or particles). Similar porous layers in the oxide scale of the $Ti_3AlC_2$ after being oxidized at 1100 °C for 16 h have been also reported [11]. XRD patterns presented in Fig. 5 and the EDS result of the enrichment of Al in the oxidized surface confirm that $\alpha$-$Al_2O_3$ is the dominant phase in the oxide scale when oxidized for 360 s, while rutile-$TiO_2$ can be detected after being oxidized for 900 s in addition to $\alpha$-$Al_2O_3$ and $Ti_3AlC_2$ phases.

$\alpha$-$Al_2O_3$ is a fairly stable protective oxide, whose growth rate is about five orders of magnitude lower than that of $TiO_2$ during the oxidation of Ti–Al alloy [31]. As a result, $TiO_2$ outgrows $Al_2O_3$ to form a $TiO_2$ outer layer. After the formation of $TiO_2$ outer layer, Ti will diffuse quickly to the $TiO_2$ layer to form a new $TiO_2$ by reacting with the O absorbed at the surface zone of the $TiO_2$ layer. The newly formed $TiO_2$ is located mainly on top of $Al_2O_3$ layer rather than beneath the $Al_2O_3$ layer because the diffusion coefficient of O is an order of magnitude smaller than that of Ti in $TiO_2$ grain [10], which results in an outward growth of $TiO_2$ layer. Unreacted O finally diffuses to the interface between the $Al_2O_3$ layer and $Ti_3AlC_2$ substrate and reacts with $Ti_3AlC_2$ substrate. With the loss of Ti, Al and C in $Ti_3AlC_2$, the $Ti_3AlC_2$ surface moves inward. The overall reaction for the oxidation of $Ti_3AlC_2$ is,

$$4Ti_3AlC_2 + 23O_2 = 12TiO_2 + 2Al_2O_3 + 8CO_2(g) \quad (3)$$

Under low oxygen potential CO rather than $CO_2$ might form. The mass densities of $Ti_3AlC_2$, $TiO_2$, and $Al_2O_3$ are 4.25 g cm$^{-3}$ [2], 4.27 g cm$^{-3}$ [32], and 3.99 g cm$^{-3}$ [33], respectively. Thus, with the consumption of one unit volume $Ti_3AlC_2$, 0.28 unit volume $Al_2O_3$ and 1.22 unit volume $TiO_2$ will be created according to Eq. (3) and the densities of these phases, which results in 50% volume expansion in solid state and mainly outward growth of the oxide scale. Obviously, the consumption of $Ti_3AlC_2$ and subsequent formation of oxides will also lead to the withdrawal of the interface between the oxide scale and bulk $Ti_3AlC_2$. The cross-section of an oxide scale formed on a polished surface of $Ti_3AlC_2$ sample after oxidation at 1100 °C for 900 s was prepared via ion-beam cross-section polishing (JEOL SM-09010 Cross Section Polisher, Japan) and is shown in Fig. 6. The advantage of ion beam polishing is that the microstructure of the sample can be more clearly explored with less mechanical damage and deformation caused by the conventional mechanically polishing. The white flat layer consisting of $Al_2O_3$ particles represents the initial $Al_2O_3$ layer formed on the well polished flat surface of the $Ti_3AlC_2$ sample, indicated by a dashed line box. The thin $Al_2O_3$ layer is not very homogenous in thickness. The inhomogeneity in thickness may be caused by anisotropic oxidation characteristics of various grains at the polished surface. It is worth of note that the $TiO_2$ grains in the outer $TiO_2$ layer are large when the $Al_2O_3$ layer is thin or less continuous, which demonstrate the importance of a dense and continuous $Al_2O_3$ layer on the oxidation resistance. It clearly shows that the thickening direction of the oxide scale after the formation of initial $Al_2O_3$ layer is outwards. The inward thickening is caused by the consumption of $Ti_3AlC_2$ substrate due to oxidation, resulting in an inward movement of the interface

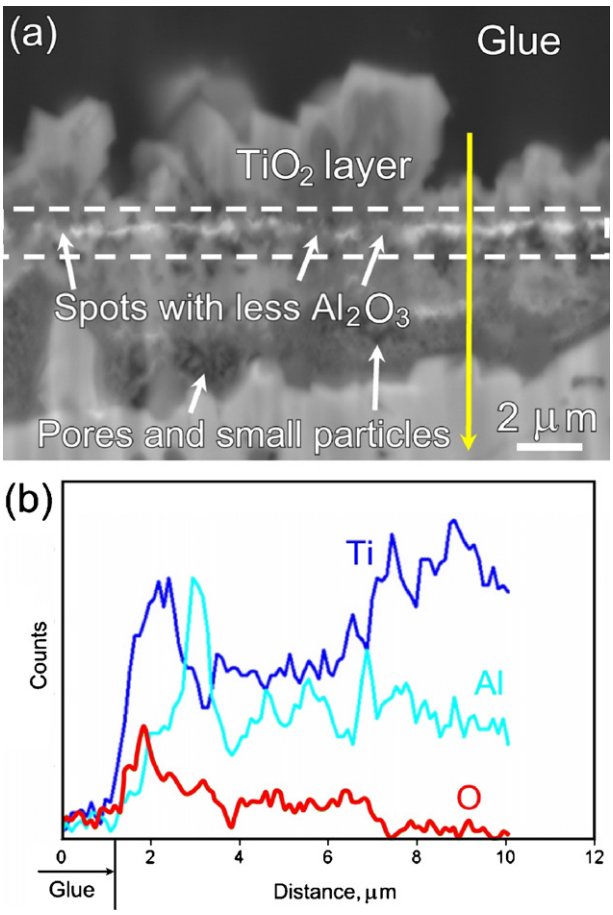


**Fig. 6.** Ion-beam polished cross-section of $Ti_3AlC_2$ ceramic oxidized at 1100 °C for 900 s (a) and the corresponding concentration profile taking along the yellow vertical line (b). The dashed box in (a) indicates the position of the initial $Al_2O_3$ layer formed on the primary flat polished surface of $Ti_3AlC_2$ substrate, showing that the thickening direction of the oxide scale after the formation of initial $Al_2O_3$ layer is both inwards and outwards.

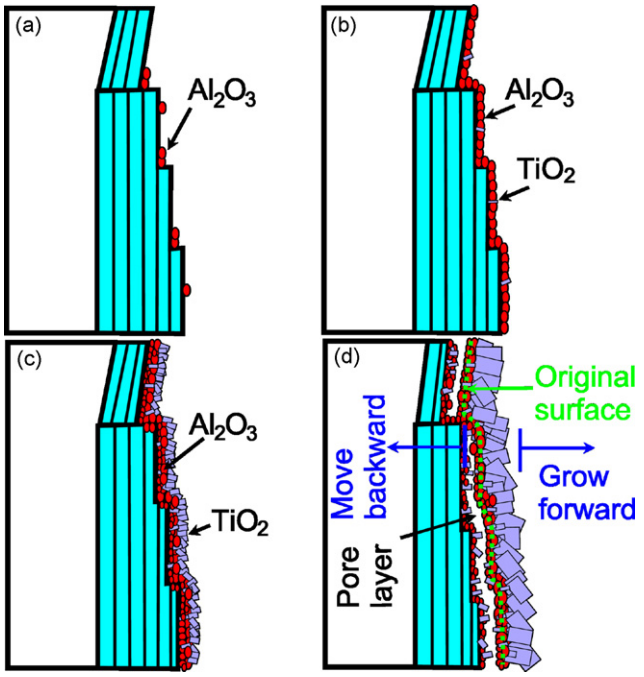


**Fig. 7.** Schematic representation of the nucleation, growth and pore formation of oxide scale on $Ti_3AlC_2$: (a) nucleation of $Al_2O_3$ on the ledges of the fractured lamellar $Ti_3AlC_2$ grains; (b) formation of $Al_2O_3$ layer and nucleation of $TiO_2$ at $Al_2O_3$ grain boundaries; (c) thickening of $Al_2O_3$ layer and outward growth of $TiO_2$ layer on $Al_2O_3$ layer; and (d) formation of porous layer once the inward grown $Al_2O_3$ can not effectively compensate the volume loss of $Ti_3AlC_2$ caused by oxidation.

between the oxide scale and $Ti_3AlC_2$ substrate. The outward diffusion of Ti leads to the formation and subsequent outward growth of $TiO_2$ outer layer. An oxidation process is schematically shown in Fig. 7. Firstly, $Al_2O_3$ nuclei formed on the ledges and surfaces of the fractured lamellar $Ti_3AlC_2$ grains, and then grow to form a thin $Al_2O_3$ layer, which results in an outward growth of the oxide scale, and meanwhile $TiO_2$ nuclei at $Al_2O_3$ grain boundaries, as shown in Fig. 7b and c. Then, the external oxygen diffuses inward through the $Al_2O_3$ layer to react with the $Ti_3AlC_2$ substrate. With the sustainable consumption of $Ti_3AlC_2$ substrate and the subsequent formation of oxides, the oxide scale/$Ti_3AlC_2$ interface withdraws, and the outward diffusion of Ti leads to the formation and subsequent outward growth of $TiO_2$ outer layer; see Fig. 7d. Once the inward grown $Al_2O_3$ cannot effectively compensate the volume loss of $Ti_3AlC_2$ caused by oxidation, a porous layer forms. The present experimental observation gives out a relative complete profile about the oxidation from oxidation starting to oxide scale thickening.

After the formation of the $Al_2O_3$ layer, if $TiO_2$ grows only on top of the $Al_2O_3$ layer and $Al_2O_3$ grows beneath the $Al_2O_3$ layer, 72 vol.% pore will unavoidably form underneath the $Al_2O_3$ layer because the formed $Al_2O_3$ can not compensate for the volume loss caused by oxidation of $Ti_3AlC_2$. Under normal circumstances pores are formed during a prolonged oxidation of $Ti_3AlC_2$ when $TiO_2$ outgrows $Al_2O_3$. The porous layer formed is a barrier for the diffusion of the further Al and Ti atoms from $Ti_3AlC_2$ substrate to $Al_2O_3$ layer and $TiO_2$ layer. Therefore, newly formed $Al_2O_3$ and $TiO_2$ particles resort on the $Ti_3AlC_2$ surface to construct an intermediate mixed ($Al_2O_3$ + $TiO_2$) layer (with $Al_2O_3$-rich inside and $TiO_2$-rich outside), as proposed by Ref. [10]. Because the $Al_2O_3$-rich band contains a lot of $TiO_2$, the Al content in this band is lower than that in the initially formed $Al_2O_3$ layer, as revealed in Figs. 6 and 8. Owing to

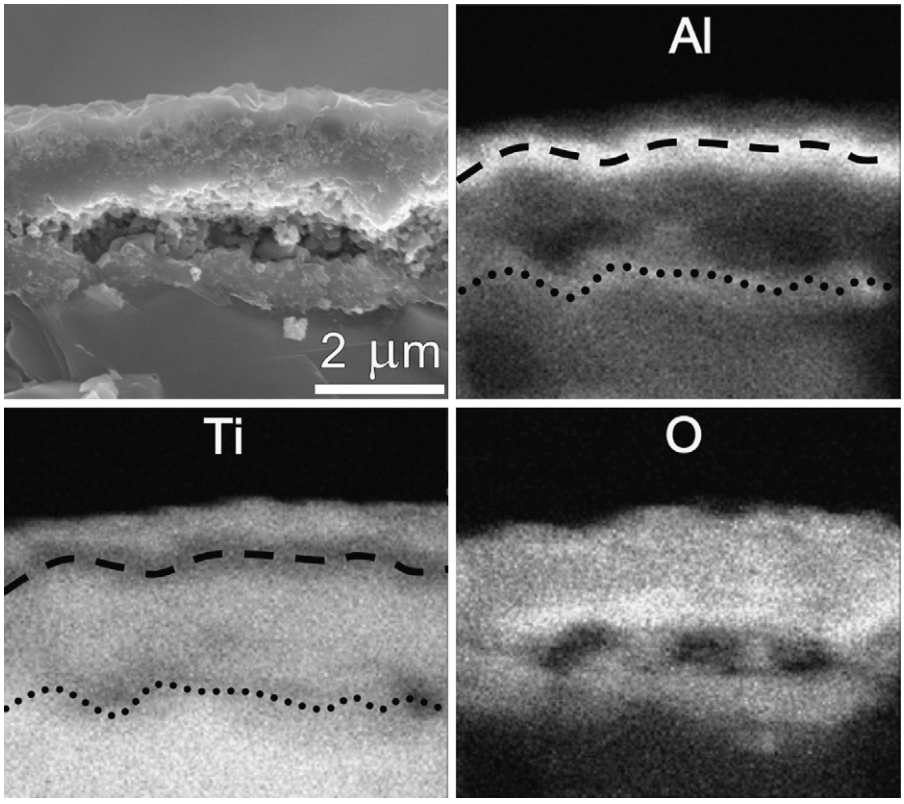


**Fig. 8.** SEM micrograph and the corresponding element maps of Al, Ti and O acquired on a fracture cross-section of the oxidized $Ti_3AlC_2$ ceramics at 1100 °C for 900 s. The dashed line shows the position of $Al_2O_3$ oxide layer initially formed at the early oxidation stage, and the dotted line shows the $Al_2O_3$-rich band adjacent to the $Ti_3AlC_2$ substrate.

the competitive nucleation and growth in the restricted area, the $TiO_2$ grains and $Al_2O_3$ grains are small. The outward growth of $TiO_2$ grains on the inner $Al_2O_3$ layer is responsible for the formation of the porous layer beneath the initial $Al_2O_3$ layer. The formation and escape of the $CO_2$ or CO further stimulates the formation of the pore layer.

## 4. Conclusion

The following conclusions can be drawn based on the findings:

(1) Predominantly $\alpha$-$Al_2O_3$ oxide nuclei form at the ledges of the fractured lamellar $Ti_3AlC_2$ grains as well as on the basal $\{0\,0\,0\,1\}$ surfaces. The $\alpha$-$Al_2O_3$ nuclei grow rapidly along these ledges and form aligned oxides. Next, they spread on the step terraces, or directly on the $\{0\,0\,0\,1\}$ basal surfaces to form an initial $Al_2O_3$ oxide layer.
(2) The formation of lenticular hexagonal pores in $Ti_3AlC_2$ grains is caused by the faster consumption of Ti, Al and C atoms along $\langle 1\,1\,\bar{2}\,0\rangle$ direction than along $\langle 0\,0\,0\,1\rangle$ direction.
(3) The thickening direction of the oxide scale after the formation of initial $Al_2O_3$ layer is both inwards and outwards. The inward thickening is caused by the consumption of $Ti_3AlC_2$ substrate due to the oxidation, resulting in an inward movement of the interface between the oxide scale and $Ti_3AlC_2$ substrate. The outward diffusion of Ti leads to the formation and subsequent outward growth of $TiO_2$ outer layer. When the formed $Al_2O_3$ cannot compensate the volume loss of $Ti_3AlC_2$ caused by oxidation, a porous layer forms underneath the $\alpha$-$Al_2O_3$ layer.

## Acknowledgement

Financial support is from the Delft Center for Materials Research Program on Self Healing Materials.

## References

[1] N.V. Tzenov, M.W. Barsoum, J. Am. Ceram. Soc. 83 (2000) 825.
[2] X.H. Wang, Y.C. Zhou, Acta Mater. 50 (2002) 3141.
[3] Y.C. Zhou, X.H. Wang, Z.M. Sun, S.Q. Chen, J. Mater. Chem. 11 (2001) 2335.
[4] H.X. Zhai, Z.Y. Huang, M.X. Ai, Y. Zhou, Z.L. Zhang, S.B. Li, J. Am. Ceram. Soc. 87 (2005) 3270.
[5] Y. Zou, Z.M. Sun, H. Hashimoto, S. Tada, Mater. Sci. Eng. A 473 (2008) 90.
[6] C.Q. Peng, C.A. Wang, Y. Song, Y. Huang, Mater. Sci. Eng. A 428 (2006) 54.
[7] J.X. Chen, Y.C. Zhou, H.B. Zhang, D.T. Wan, M.Y. Liu, Mater. Chem. Phys. 104 (2007) 109.
[8] J.X. Chen, Y.C. Zhou, Oxid. Met. 65 (2006) 123.
[9] G.M. Song, Y.T. Pei, W.G. Sloof, S.B. Li, J.T.M. De Hosson, S. Van der Zwaag, Scripta Mater. 58 (2008) 13.
[10] M.W. Barsoum, J. Electrochem. Soc. 148 (2001) C544.
[11] M.W. Barsoum, N. Tzenov, A. Procopio, T. El-Raghy, M. Ali, J. Electrochem. Soc. 148 (2001) C551.
[12] X.H. Wang, Y.C. Zhou, Corros. Sci. 45 (2003) 891.
[13] X.H. Wang, Y.C. Zhou, Chem. Mater. 15 (2003) 3716.
[14] X.H. Wang, Y.C. Zhou, Mater. Res. Innovat. 7 (2003) 381.
[15] Z.M. Sun, Y.C. Zhou, M.S. Li, Corros. Sci. 43 (2001) 1095.
[16] Y.C. Zhou, H.Y. Dong, X.H. Wang, Oxid. Met. 61 (2004) 365.
[17] L.F. He, Y.C. Zhou, Y.W. Bao, J.Y. Wang, M.S. Li, Int. J. Mater. Res. 98 (2007) 3.
[18] Y.W. Bao, C.F. Hu, Y.C. Zhou, Mater. Sci. Technol. 22 (2006) 227.
[19] X.M. Min, Y. Ren, J. Wuhan, Univ. Technol.—Mater. Sci. 22 (2007) 27.
[20] Y.C. Zhou, Z.M. Sun, X.H. Wang, S.Q. Chen, J. Phys.: Condens. Matter 13 (2001) 10001.
[21] D. Legzdina, I.M. Robertson, H.K. Birnbaum, Acta Mater. 53 (2005) 601.
[22] D.R. Lide, Handbook of Chemistry and Physics, 76th ed., CRC Press, New York, 2000, pp. 5–72.
[23] TWC4 Software, Thermo-Calc Software AB, Sweden, 2006, www.thermocalc.com.
[24] G. Palasantzas, J.T.M. De Hosson, Phys. Rev. E 67 (2003) 021604.
[25] X.H. Wang, Y.C. Zhou, J. Mater. Chem. 12 (2002) 2781.
[26] Z.J. Lin, M.J. Zhou, Y.C. Zhou, M.S. Li, J.Y. Wang, J. Am. Ceram. Soc. 89 (2006) 2964.
[27] Z.J. Lin, M.J. Zhou, Y.C. Zhou, M.S. Li, J.Y. Wang, Scripta Mater. 54 (2006) 1815.
[28] A. Bellucci, D. Gozzi, Chem. Mater. 15 (2003) 1217.
[29] K. Tang, C.A. Wang, Y. Huang, Q.F. Zan, J. Cryst. Growth 222 (2001) 130.
[30] T. Goto, T. Hirai, Mater. Res. Bull. 22 (1987) 1199.
[31] M.R. Yang, S.K. Wu, Bull. College Eng. N. T. U. 89 (2003) 3.
[32] H. Shintani, S. Sato, Y. Saito, Acta Crystallogr., Sect. B 31 (1975) 1981.
[33] Y. Zhou, Ceramic Materials, Press of Harbin Institute of Technology, Harbin, 1996.